EPJ Appl. Metamat. **9**, 12 (2022)
© Y.B. Habibullah and T. Ishihara, Published by EDP Sciences, 2022
https://doi.org/10.1051/epjam/2022013

EPJ Applied Metamaterials

Available online at:
epjam.edp-open.org

Metamaterials for Novel Wave Phenomena in Microwaves, Optics, and Mechanics

RESEARCH ARTICLE OPEN ACCESS

The role of nonlocal response in second harmonic generation at metasurfaces with triangular metaatoms

Yusuf B. Habibullah and Teruya Ishihara*

Tohoku University, Department of Physics, Graduate School of Science, 6–3 Aramaki-Aoba, 980–8578 Sendai, Japan

Received: 21 November 2021 / Accepted: 26 April 2022

Abstract. Metasurface consisting of square array of obtuse isosceles triangle metaatoms is found to exhibit much more efficient second harmonic generation (SHG) compared to that of split ring resonators and its heptagonal modification, experimentally as well as numerically. All of them are designed to lack inversion symmetry in horizontal direction but to have vertical symmetry, and to meet the double resonance condition for vertically-polarized fundamental and horizontally-polarized SHG waves. SHG efficiencies were estimated numerically for each structure by evaluating an overlap integral of second order nonlinear polarization and field distribution at the SHG wavelength. The large overlap integral for the triangle metasurface is ascribed to the nonlocal response at the SHG wavelength. Current induced at the center of the triangle near the obtuse angle by horizontally polarized light at SHG wavelength flows toward two corners of acute angles. As a result, polarization charges oscillate in time at the surfaces of two acute corners, which results in strong field oscillation away from the center where the electric field is applied to majority of free electrons. Experimentally observed wavelength dependence of SHG efficiencies for the three metasurfaces are reasonably reproduced by a numerical estimation.

1 Introduction

Response of material to the electric field of light at one point can be determined not only by an electric field at the point but also the electric field at the other points around it. This effect, nonlocality, has not got much attention but known to have some detectable effects [1–3]. In the context of nonlinear optics, nonlocality has been discussed for a second harmonic generation (SHG) in a metallic sphere by expanding electric field in terms of multipoles [4]. There are several review papers on nonlocal effects on nonlinear optical processes described with a hydrodynamic equation, where the origin of nonlocality is ascribed to gradient of electron density [1,2,5]. Another type of nonlocal response arises in metamaterials when effective permittivity depends on wavevector, which can be calculated using a Green's function [6].

In this paper we investigate SHG from metasurfaces consisting of artificially fabricated Au particles that lack inversion symmetry in horizontal x–direction for normal incidence. We assume that the electron density is constant throughout the metal. Therefore, the nonlocality which has been discussed in some of the literatures does not play any role. Instead, we pay attention to the electron flow induced by electric field or time-varying magnetic field in the asymmetric-shaped isolated metal "particles" or metaatoms. Due to charge conservation, the current induces charges at the surface of metaatom, which generate electric field at the point far from the point of excitation. This electric field on the surface contributes to SHG at far-field if symmetry of the metaatom allows.

In order to discuss this effect, we employ an overlap integral, which was initially introduced empirically to characterize efficiency of SHG [7–9]. Later it was pointed out that the formula can be derived rigorously from Lorentz reciprocity [10] and applied to metamaterials [11]. Since then, there are quite a few papers using this formula to discuss SHG from metasurfaces [12,13].

Figure 1 shows schematic configuration considered in this paper. Only one unit cell is shown for simplicity. The unit cells are arranged periodically both horizontal (x) and vertical (y) directions. The incident light propagates toward negative z-direction and SHG is detected in the transmission configuration. The unit cell consists of a Au particle with a particular asymmetric shape.

SHG field amplitude at far field is given [11] by

$$E_{\mathrm{SHG}} \propto \int\int E_{\perp}^{x,2\omega}(\boldsymbol{r}) P_{\perp}^{(2)y}(\boldsymbol{r}) dS, \tag{1}$$

where $P_{\perp}^{(2)y} = \chi_{\mathrm{S},\perp\perp\perp}^{(2)} E_{\perp}^{y,\omega}(\boldsymbol{r}) E_{\perp}^{y,\omega}(\boldsymbol{r})$ is the normal component of the second order nonlinear surface polarization excited by y-polarized light of the fundamental

* e-mail: t-ishihara@tohoku.ac.jp

This is an Open Access article distributed under the terms of the Creative Commons Attribution License (https://creativecommons.org/licenses/by/4.0), which permits unrestricted use, distribution, and reproduction in any medium, provided the original work is properly cited.

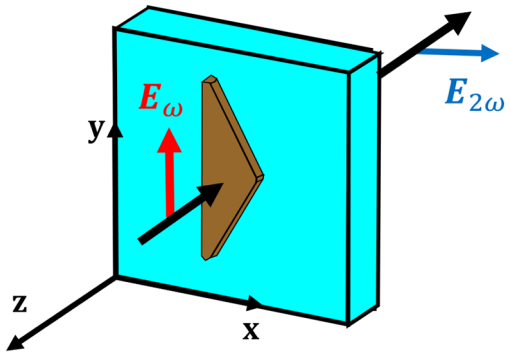

Fig. 1. Schematic configuration for SHG emission considered in this paper. Fundamental light with y-polarization is normally incident on the metasurface. Transmitted SHG with x-polarized is observed.

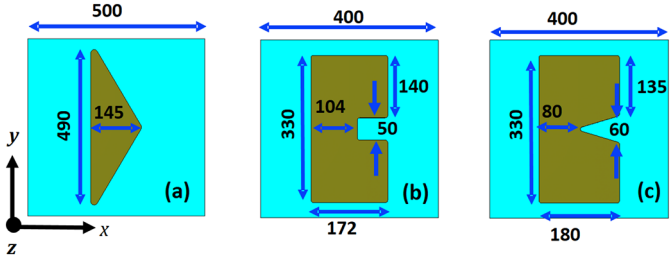

Fig. 2. Unit cell structures of metaatoms discussed in this work: (a) Triangle, (b) SRR, and (c) Heptagon. Size parameters are in nm. The size parameters define the structure before rounding the corners with radius of 10 nm.

wavelength. Here the normal component of a vector field $\boldsymbol{A}(\boldsymbol{r})$ is defined by $A_\perp(\boldsymbol{r}) \equiv \boldsymbol{A}(\boldsymbol{r})\cdot\boldsymbol{n}(\boldsymbol{r})$, where $\boldsymbol{n}(\boldsymbol{r})$ is the normal vector of a surface at $\boldsymbol{r}$. $\boldsymbol{E}^{y,\omega}(\boldsymbol{r})$ and $\boldsymbol{E}^{x,2\omega}(\boldsymbol{r})$ are the local electric field excited by y-polarized fundamental and x-polarized SHG plane waves, respectively. Note that $\boldsymbol{E}^{y,\omega}(\boldsymbol{r})$ is not necessarily parallel to the direction of excitation y, nor is $\boldsymbol{E}^{x,2\omega}(\boldsymbol{r})$ to x-direction. We take only $\chi^{(2)}_{S,\perp\perp\perp}$ into account as it is known to be dominant [14–16]. Also note that SHG amplitude at far field is not given by the integral of nonlinear polarization itself but by the overlap integral with electric field for the SHG wavelength excitation over the surface. Therefore, in order to find a design for efficient SHG, one need to know the field distributions at the metal surface both at the fundamental and SHG wavelengths.

In our previous work [17], we experimentally investigated SHG from three metasurfaces. Based on the shape of the particles in their unit cell, we refer them to Triangle, SRR (split ring resonator) and Heptagon structures, respectively hereafter. As the fundamental wavelength were varied, all of them exhibited resonant enhancement of SHG, among which the Triangle structure had the most efficient conversion. In this paper, we are going to explain why the triangle structure was the most efficient, which will be ascribed to nonlocal response of the structure.

2 Metasurface design and characterization

Figure 2 shows three of unit cell designs for our investigation with their characteristic lengths. All the designs have a square unit cell with one isolated gold metaatoms in it. The surface chemical stability and non-toxicity of gold makes it a plasmonic material of our choice. We determined these parameters so that each structure has a fundamental resonance at 1360 nm and SHG resonance at 680 nm by using parameter scan with a commercial electromagnetic numerical calculation package (CST Studio Suite) with periodic boundary conditions. The designs were achievable by taking the full advantage of the polarization orthogonality of the resonant positions at fundamental and SH wavelengths. Permittivity of Au was taken from [18]. For the SRR and the Heptagon, it is easy to find appropriate structural parameters, as resonance for x-polarization is almost independent of the size in y-direction, which was the reason why we chose cross-polarized double resonance geometry. As for the Triangle, it turned out that it was more challenging as they are dependent. The calculated transmission for the three designs is shown in Figure 3. Prominent transmission dips at 1360 nm are their lowest (in terms of frequency) resonances for y-polarization. For x-polarization, the SRR and the Heptagon design have well developed lowest resonances at 680 nm, while for the triangle, we were only able to tune parameters to match the resonance at the second lowest transmission dip, which is less prominent than the lowest. The unit cell size is 500 nm for the Triangle with the metaatom thickness of 32 nm, while 400 nm for the SRR and the Heptagon structures with thickness of 40 nm. In order to minimize size fluctuations in fabrication process, we employed a Focused Ion Beam (FIB) machine to engrave the pattern (rather than Electron Beam lithography technique) on thin platelet single crystals (rather than deposited film) of Au. Details of sample fabrication is described in [17].

3 SHG spectra

Once a unit cell design is determined, it is possible to predict SHG efficiency as a function of the incident wavelength λ from the overlap integral as we mentioned earlier. In order to make a fair comparison for SHG amplitude for different unit cell size, we introduce a figure of merit (FOM) for y-polarized excitation and x-polarized SHG emission as

$$\eta_{xyy}(\lambda) = \frac{\iint E_\perp^{x,2\omega}(\boldsymbol{r}) E_\perp^{y,\omega}(\boldsymbol{r}) E_\perp^{y,\omega}(\boldsymbol{r})}{E_0^3} \frac{dS}{L_x L_y}, \qquad (2)$$

where $L_x L_y$ is the unit cell size of the metasurface, E_0^3 is the cube of the amplitude of the input light on the metasurface, and $E_\perp^{y,\omega}(\boldsymbol{r})$ is the normal component of the local electric field vector upon y-excitation at ω frequency and $E_\perp^{x,2\omega}(\boldsymbol{r})$ is the normal component of local electric field vector excited by an x-polarized hypothetical plane wave from the observation point at 2ω frequency [11]. We dropped a surface nonlinear susceptibility as it is common to all three

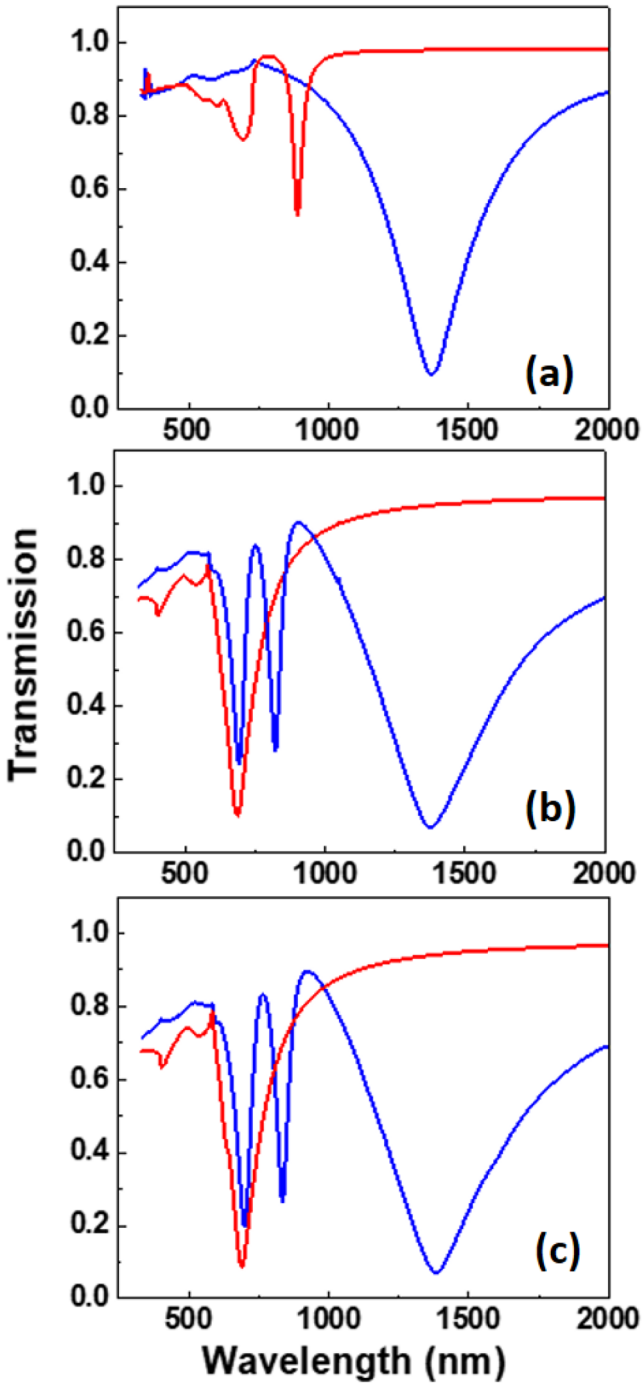

Fig. 3. Calculated transmission spectra for y-polarized (red) and x-polarized (blue) lights for (a) Triangle, (b) SRR and (c) Heptagon structures.

structures. In general, the integral is carried out over the surface of the particle, but in our case only over "side walls" of metaatoms, where the normal vector is on xy-plane, as the experiments were carried out for normal incidence. Upon calculation it turned out that the integral is dependent on the phase relation between the two fields. We chose the phase at each wavelength so that the integral gives maximum value.

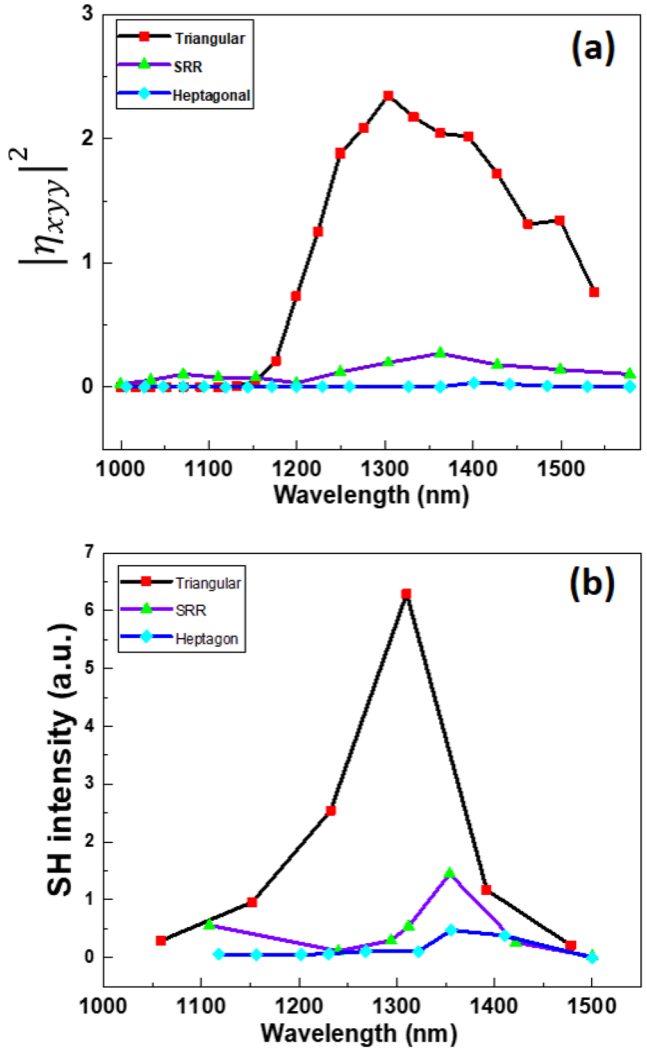

Fig. 4. Comparison of SHG intensity as a function of fundamental wavelength. (a) Numerical calculation, (b) Experimental measurement.

Figure 4a shows square of FOM, which is proportional to the SHG intensity at far field, for three metasurfaces, as a function of the fundamental wavelength. In spite of the less prominent resonance seen at the SHG wavelength for the Triangle in Figure 3a, the Triangle exhibits by far efficient SHG. In order to confirm the tendency in experiment, we measured the SHG emission from our samples excited by a tunable light source. The detail of the experiments is described in [17]. Wavelength dependence of the SHG intensity obtained in the experiments is shown in Figure 4b. All three structures exhibit resonance at the wavelength of the double resonance, among which the Triangle structure exhibits much more efficient SHG compared to the SRR and the Heptagon, reproducing numerical calculations. In order to understand the reason, let us investigate (numerically calculated) field distribution in three designs.

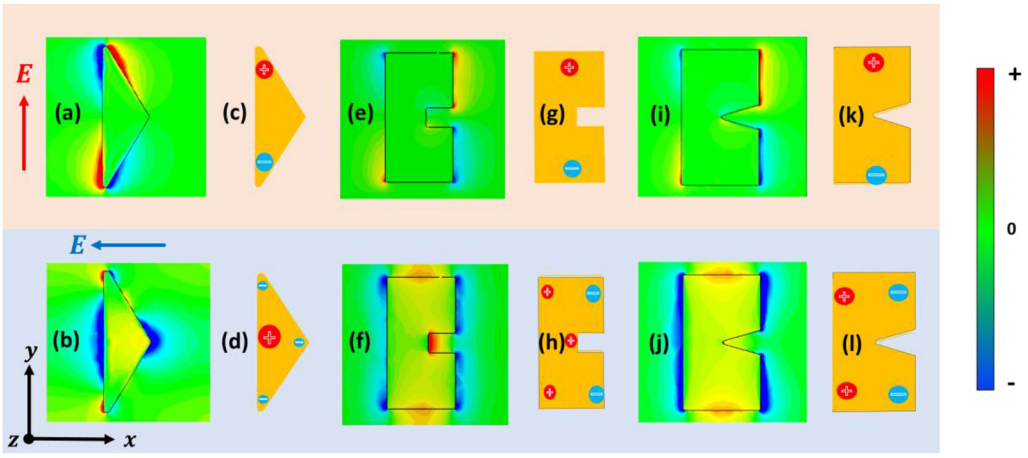

Fig. 5. E_x distrubutions in unit cells of Triangle (a,b), SRR (e,f) and Heptagon (i,j) structures at fundamental and SHG resonance, respectively. Corresponding schematic charge distribution in unit cell of Triangle (c,d), SRR (g,h) and Heptagon (k.l) structures. See Supplementary Material for dynamic version of (a) and (b) and corresponding E_y distributions.

4 Discussion

Figure 5 shows pseudo-color presentation for the x-component of microscopic electric field E_x in unit cells for three structures at a particular moment when its pattern is most characteristic at resonances (1360 nm for y-polarized excitation and 680 nm for x-polarized excitation). (See Supplementary Material for dynamic versions of (a) and (b) and corresponding E_y distributions.) In the case of the Triangle, strong E_x field is located at the two acute corners of a triangle for y-excitation as is shown in (a). At this moment, at the upper corner of the triangle, positive charge is accumulated in the metal. As a result, this part becomes a source of electric field. On the right side of the upper corner, electric field points to the positive direction, which is presented as red, while on the left side of the corner it points to the negative direction, which is presented as blue. After half a cycle, this part becomes a drain of electric field and the color flips. For x-excitation, at the middle of the triangle, both right and left sides of the triangle are attached to blue color regions suggesting the same sign for E_x, resulting in opposite sign of charge accumulated on the opposite sides. At the two acute angles, however, E_x direct to the opposite directions, which correspond to negative charge at this moment. As the integrand of the overlap integral is $E_{\perp}^{x,2\omega}(\boldsymbol{r})\left(E_{\perp}^{y,\omega}(\boldsymbol{r})\right)^2$,the sign for the fundamental field does not matter, while that of the SHG field does matter. Therefore these field overlaps at the acute corners contribute constructively to the SHG. On the other hand, for the SRR and the Heptagon, for x-polarization, E_x at the both sides of acute corners have the same direction, which corresponds to opposite sign of normal component. Thus these overlaps on the other sides cancell to each other. This is the reason why the Triangle has much larger SHG intensity compared to the SRR and the Heptagon.

Now let us consider why the Triangle exhibits such a characteristic field distribution. The E_x distribution suggests that at the acute corners, a net charge oscillates in time, which is not possible if this part was isolated. But as a matter of fact, this part is connected to the center part of the triangle, where electrons are shaken by the x-polarized light. In order to understand this process, let us look at the current distribution inside the triangle.

Figure 6 shows the current distributions for y-polarized excitation at the fundamental resonance and x-polarized excitations at the SHG resonance for three metasurfaces. (See Supplementary Material for a dynamic version of this figure.) They are calculated by solving Maxwell equations for given material arrangements. Note that no nonlinearity is considered at this stage. Nonlinearity arises when overlap integral is evaluated. In addition to the main stream of the current in the middle, we notice substreams toward the two acute corners. As the current cannot flow any further at the end of corners, it generates polarization charge on the surface, which results in electric field concentration there. Thus the electric field induces current flow at the middle of the triangle, which results in charge accumulation at different points, which can be referred to as a nonlocal response. And this nonlocal response is responsible for the large overlap of the nonlinear polarization and the SHG field, which gives efficient SHG at far field. Note that in this discussion, we did not consider any charge density gradient in the bulk, which has been discussed as an origin of nonlocality [1,2,5]. If the shape of the metaatom allows (if it breakes inversion symmetry), this oscilation contributes to the SHG at the farfield. In order to make comparison, current distribution for the SRR and the Heptagon are shown in Figure 5e,f,i,j and corresponding charge distribution are schematically displayed in Figure 5g,h,k,l. For example, as is clear from Figure 5f,j for x-excitation at the SHG resonance, current flows from the left side to the right side, which results in E_x with the same direction. As the two faces have opposite normal vectors, they cancel to each other in the overlap integral, although there are considerable mode overlap. Our argument was made for metasurfaces with just a few types of single particles in a unit cell. Extending this approach to previous discussions on other shapes or composite metaatoms [19–26] may help general understanding of SHG in metaatoms.

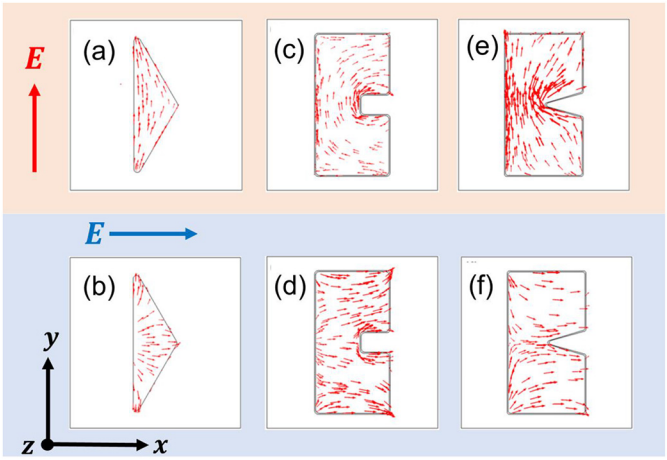

Fig. 6. Inplane arrow plots showing direction of current for Triangle (a,b), SRR (c,d) and Heptagon (e,f) structures at fundamental and SHG resonance, respectively. See Suplementary Material for a dynamic version of this figure.

5 Conclusion

In an obtuse isosceles triangle metaatom optimized for double resonance, SHG is generated efficiently due to the nonlocal response, which is originated from the characteristic current flow in this isolated metaatom. The fundamental light with x-polarized light shakes majority of electrons in the middle part to generate current flow to the two acute corners of the triangle, which guarantee constructive contribution to the overlap integral with the second order nonlinear polarization induced by y-polarized excitation at the fundamental wavelength. Our results contribute to the understanding of the linear and nonlinear optical properties of resonant plasmonic metasurfaces and open a way for the efficient nanoscale nonlinear medium with potential application in photonic integrated nano-circuitry and nano-optoelectronics.

Supplementary Material

Fig. S1. Time evolution of E_x and E_y distrubutions in a unit cell of Triangle at (a) fundamental and (b) SHG resonance, respectively.
Fig. S2. Dynamic version of Figure 6. Inplane arrow plots showing direction of current for Triangle (a,b), SRR (c,d) and Heptagon (e,f) structures at fundamental and SHG resonance, respectively.

The Supplementary Material is available at https://epjam.edp-open.org/10.1051/epjam/2022013/olm.

This work was partially supported by Nohmura Foundation for Membrane Structure's Technology.

References

1. S. Raza, S.I. Bozhevolnyi, M. Wubs et al., Nonlocal optical response in metallic nanostructures, J. Phys.: Condens. Matter **27**, 183204 (2015)
2. T. Christensen, W. Yan, S. Raza et al., Nonlocal response of metallic nanospheres probed by light electrons, and atoms, ACS Nano **8**, 1745 (2014)
3. B. Gallinet, J. Butet, O.J.F. Martin, Numerical methods for nanophotonics: standard problems and future challenges, Laser Photonics Rev. **9**, 577 (2015)
4. J.I. Dadap, J. Shan, T.F. Heinz, Theory of optical second-harmonic generation from a sphere of centrosymmetric material: small-particle limit, J. Opt. Soc. Am B **21**, 1328 (2004)
5. A.V. Krasavin, P. Ginzburg, A.V. Zayats, Free-electron optical nonlinearities in plasmonic nanostructures: a review of the hydrodynamic description, Laser Photonics Rev. **12**, 1700082 (2018)
6. M.A. Gorlach, T.A. Voytova, M. Lapine et al., Nonlocal homogenization for nonlinear metamaterials, Phys. Rev. B **93**, 165125 (2016)
7. L. Carletti, A. Locatelli, O. Stepanenko et al., Enhanced second-harmonic generation from magnetic resonance in AlGaAs nanoantennas, Opt. Express **23**, 26544 (2015)
8. M. Celebrano, X. Wu, M. Baselli et al., Mode matching in multiresonant plasmonic nanoantennas for enhanced second harmonic generation, Nat. Nanotechnol. **10**, 412 (2015)
9. B.-L. Wang, R. Wang, R.J. Liu et al., Origin of shape resonance in second-harmonic generation from metallic nanohole arrays, Sci. Rep. **3**, 2358 (2013)
10. S. Roke, M. Bonn, A.V. Petukhov, Nonlinear optical scattering: the concept of effective susceptibility, Phys. Rev. B **70**, 115106 (2004)
11. K. O'Brien, H. Suchowski, J. Rho et al., Predicting nonlinear properties of metamaterials from the linear response, Nat. Mater. **14**, 379 (2015)
12. J. Butet, O.J.F. Martin, Evaluation of the nonlinear response of plasmonic metasurfaces: Miller's rule, nonlinear effective susceptibility method, and full-wave computation, J. Optic. Soc. Am. B **33**, A8 (2016)
13. A. Noor, A.R. Damodaran, I.-H. Lee et al., Mode-matching enhancement of second-harmonic generation with plasmonic nanopatch antennas ACS, Photonics **7**, 3333 (2020)
14. D. Krause, C.W. Teplin, C.T. Rogers et al., Optical surface second harmonic measurements of isotropic thin-film metals: gold silver, copper, aluminum, and tantalum, J. Appl. Phys. **96**, 3626 (2004)

15. B. Wang, T. Koschny, C.M. Soukoulis, Wide-angle and polarization-independent chiral metamaterial absorber, Phys. Rev. B **80**, 033108 (2009)
16. G. Bachelier, J. Butet, I. Russier-Antoine et al., Origin of optical second-harmonic generation in spherical gold nanoparticles: local surface and nonlocal bulk contributions, Phys. Rev. B **82**, 235403 (2010)
17. Y.B. Habibullah, T. Ishihara, Comparison of second harmonic generation from cross-polarized double-resonant metasurfaces on single crystals of Au, Nanophotonics **11**, 1931 (2022)
18. P.B. Johnson, R.W. Christy, Optical constants of the noble metals, Phys. Rev. B **6**, 4370 (1972)
19. B.K. Canfield, H. Husu, J. Laukkanen et al., Local field asymmetry drives second-harmonic generation in noncentrosymmetric nanodimers, Nano Lett. **7**, 1251 (2007)
20. V.K. Valev, X. Zheng, C.G. Biris et al., The origin of second harmonic generation hotspots in chiral optical metamaterials [Invited], Optic. Mater. Express **1**, 36 (2011)
21. A. Salomon, M. Zielinski, R. Kolkowski et al., Size and shape resonances in second harmonic generation from silver nanocavities, J. Phys. Chem. C **117**, 22377 (2013)
22. R. Czaplicki, J. Mäkitalo, R. Siikanen et al., Second-harmonic generation from metal nanoparticles: resonance enhancement versus particle geometry, Nano Lett. **15**, 530 (2015)
23. R. Hou, V. Shynkar, C. Lafargue et al., Second harmonic generation from gold meta-molecules with three-fold symmetry, Phys. Chem. Chem. Phys. **18**, 7956 (2016)
24. S.D. Gennaro, M. Rahmani, V. Giannini et al., The interplay of symmetry and scattering phase in second harmonic generation from gold nanoantennas, Nano Lett. **16**, 5278 (2016)
25. M.A. Gorlach, D.A. Dobrykh, A.P. Slobozhanyuk et al., Nonlinear symmetry breaking in photometamaterials, Phys. Rev. B **97**, 115119 (2018)
26. K.Y. Raygoza-Sánchez, I. Rocha-Mendoza, P. Segovia et al., Polarization dependence of second harmonic generation from plasmonic nanoprism arrays, Sci. Rep. **9**, 11514 (2019)

Cite this article as: Yusuf B. Habibullah, Teruya Ishihara, The role of nonlocal response in second harmonic generation at metasurfaces with triangular metaatoms, EPJ Appl. Metamat. **9**, 12 (2022)